Assessing Environmental Impact of STOL Takeoff: A Computational Analysis of Geometric Modifications on Airfoils

Kumudha Srinivas

Abstract |

The aviation industry is responsible for roughly 950,000 metric tonnes of annual CO_2 emissions, as well as having contributed to 4% of global warming as of 2024 [1]. But as society transitions to prioritizing sustainability, the global aviation industry is faced with increasing pressure to decarbonize. A critical aspect of this larger “green aviation” agenda is the mission of minimizing fuel burn from aircraft’s energy-intensive phase of takeoff and climbing. Although they have experimented with various ‘green’ designs - which use systems such as blown lift technologies (which employ distributed electric fans on the wings) [2], bio-fuels, and electric and hybrid engines [3]- engineers are still conducting research to determine the best ways to optimize aircraft efficiency, and in turn, aircraft sustainability. Notably, the Short Take-Off and Landing (STOL) capable aircraft design poses a particular challenge. STOL aircraft are fixed-wing aircraft that can take off and land on runways that are a lot shorter in length than the ones used for conventional aircraft [4]. This allows aircraft to operate in areas without the traditional lengthy runways - areas that conventional aircraft might not be able to reach. This opens up the opportunity to connect isolated communities and remote, unpredictable terrain to the outside world. Since STOL aircraft take off from significantly shorter runways, they are required to accelerate to liftoff speed incredibly rapidly, which demands a massive surge of engine power. This aggressive acceleration forces traditional STOL designs to burn a disproportionate amount of fuel in just a matter of seconds, highlighting the urgent need to structurally optimize aircraft to be inherently more efficient at translating engine power into aerodynamic lift [5]. This issue leads us to examine a vital aspect of aircraft wing design that dictates how the aircraft interacts with moving air to keep the machine airborne: the airfoil. How do geometric modifications on airfoils affect the lift-to-drag ratio of an aircraft, and to what extent can these changes optimize takeoff capability and reduce the carbon footprint of STOL aircraft?

Introduction |

To start, we must understand exactly what an airfoil is and how it contributes to the flight of an aircraft. An airfoil is essentially a streamlined shape (airplane wing or propeller blade) that is designed to generate lift (also known as thrust) when air is flown over it - a geometric cross section of the wing [6]. The purpose of an airfoil is to reduce drag and generate lift. However, each individual design for different airfoils will vary for each use case. For instance, airfoils for aircrafts operating at high altitudes often feature a highly concave curve on the bottom and an intense arch at the top, whereas low-altitude airfoils have a more mild camber. The different parts of and terminology about any given airfoil are as follows:

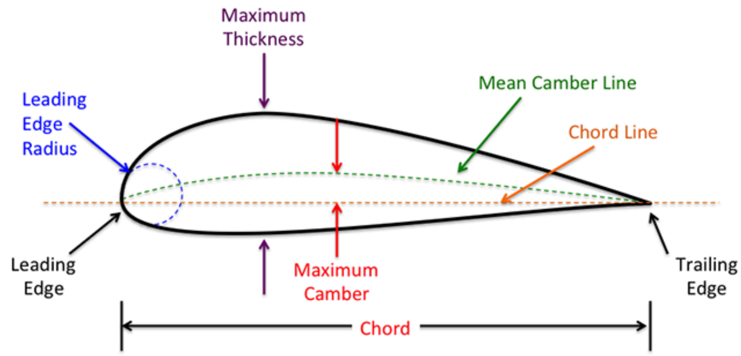

Figure 1: Parts of an airfoil [7]

Term	Definition
Chord Line	Theoretical line between the leading and trailing edges (front-most and rear edges) of an airfoil.
Camber	Slightly convex or arched shape of a horizontal surface - curvature
Mean Camber Line	Centerline between upper and lower surfaces
Maximum Camber	Maximum vertical distance between Chord Line and Mean Camber Line
Maximum Thickness	Maximum vertical distance between lower surface and upper surface of the airfoil
Upper Surface Camber	Curve at the top of an airfoil (typically more curved than the lower surface)
Lower Surface Camber	Curve at the bottom of an airfoil
Angle of Attack	Angle between the chord line and the flow direction
Relative Wind	Airflow relative to an airfoil, that is created by the movement of the airfoil. EX: A wing moving at 100 mph will create relative wind that moves in the opp. Direction at 100 mph, over and under the wing

The specific shape of the airfoil will enable efficient movement through a given fluid through the manipulation of pressure difference - faster air over the curved top of the airfoil, and slower air below, creating a net upward force. Typically, aerodynamic lift can be explained with two underlying explanations: Bernoulli's Principle of Pressure and Newton's Third Law [8]:

1. Bernoulli's Principle of Pressure: When the airfoil moves through the fluid, the shape causes an increase in the air's velocity across its upper surface. This, in turn, results in a drop in pressure in the area above the airfoil and an increase in pressure below. This is what generates the lift force.
2. Newton's Third Law: This explanation focuses less on the velocity of the air, and more on its fluidity. The moving airfoil essentially shifts the air around it, the air moving upwards over the airfoil is an upwash, and the air below is downwash. The pressure difference between the upwash and downwash generates lift by turning the incoming air downwards.

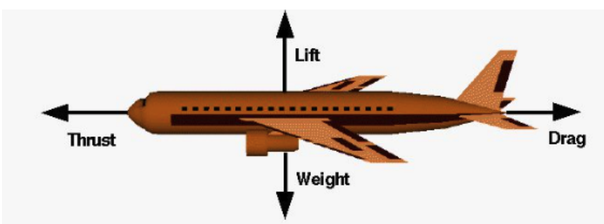

Figure 3: Four forces of flight [9]

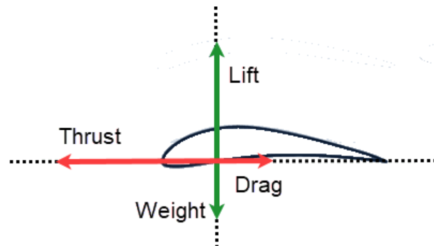

Figure 4: Four forces of flight [9]

According to Bernouli's equation, the change in velocity leads to a change in pressure relative to the local atmospheric pressure.

$$P_2 - P_1 = -\frac{1}{2}\rho(U_2^2 - U_1^2)$$

P is the static pressure

ρ is the density of the fluid medium

U is the fluid velocity

Equation 1: Bernouli's Equation [10]

As the air flows above the top surface of the airfoil, it accelerates across the curve. Since the pressure on top of the surface (P2) would then be less than the freestream pressure (P1), a suction is created on the top surface, pulling the airfoil upwards and contributing towards lift.

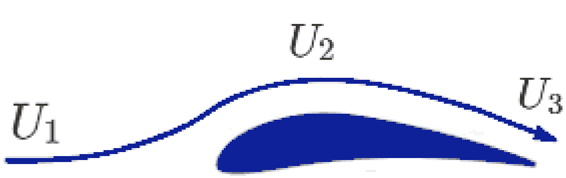

Figure 5: Air velocity above airfoil [9]

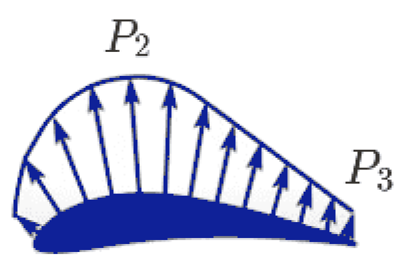

Figure 6: Pressure distribution above airfoil [9]

Similarly, the airflow around the bottom surface also contributes to pressure differences and generating lift. In the airfoil depicted below, U2 is when the velocity of the air increases (airflow accelerates), causing a suction pressure that pulls the airfoil downwards initially. However, as the air moves further along the bottom, the flow decelerates (the curvature changes) and causes an increase in the pressure. Since this pressure would be higher than the local atmospheric pressure, lift will be generated.

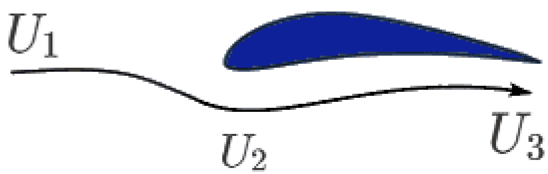

Figure 7: Air velocity below airfoil [9]

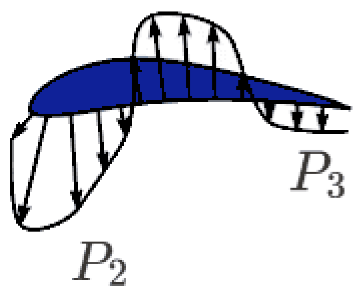

Figure 8: Pressure distribution below airfoil [9]

While maximizing lift is essential for aerodynamic flight, every cycle of lift generation by an airfoil also inherently produces an opposing force: drag. The relationship between these two forces can be mathematically expressed as the lift-over-drag ratio (L/D ratio), which also serves as a metric for an airfoil's overall aerodynamic efficiency [11].

In terms of environmental impact, the L/D ratio of an aircraft is inversely proportional to fuel consumption. When an airfoil has a low L/D ratio, the engines burn a disproportionately higher amount of fuel to produce the thrust needed to overcome the excessive drag. On the other hand, a maximized L/D ratio ensures that the aircraft gains the most thrust it can for a low amount of air resistance, directly reducing fuel consumption and carbon emissions [11].

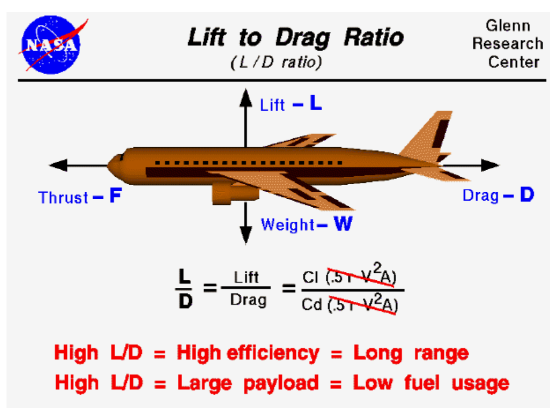

Figure 9: Lift to Drag Ratio [11]

This ratio is not a fixed number; instead, it is completely dictated by the design and shape of the airfoil. Altering specific parameters of an airfoil can manipulate how air molecules move across the upper and lower surfaces. Through these geometric modifications, engineers can customize an airfoil's shape and maximize its L/D ratio for its respective use case.

For conventional aircrafts, airfoils are optimized primarily for high-speed cruise efficiency, which would typically be achieved by maximizing the lift coefficient [12].

$$Cl = \frac{L}{r \bullet \frac{v^2}{2} \bullet A}$$

Equation 2: The Lift Coefficient [13]

For STOL aircrafts, however, the performance criteria becomes generating immense lift within a drastically shortened runaway at low-speed velocities.

During takeoff, an aircraft's total drag comprises ground friction and aerodynamic drag. If an airfoil were to generate high lift while also creating excessive drag (a low L/D ratio), it would act as a hindrance to the initial acceleration phase [14]. Maximizing the L/D ratio ensures that the wing generates the necessary lift without also facing a high drag that would restrict the aircraft from accelerating rapidly. Furthermore, a maximized L/D ratio would also help the STOL aircraft gain altitude fast over obstacles beyond the short runway. In flight mechanics, the steady climb angle is directly controlled by the the thrust-to-weight ratio and the inverse of the L/D ratio:

$$sin(y) = (T/W) - ((1)/(L/D))$$

Equation 3: Climb angle in terms of L/D ratio [15]

Since a higher L/D ratio would directly increase the climb angle for a given thrust, a maximized L/D ratio would allow the STOL aircraft to clear surrounding obstacles such as trees, buildings, or hills, at the end of a short runway while also requiring less engine thrust.

Thus, a STOL airfoil must be designed to maximize not the lift coefficient, but the L/D ratio.

Methodology |

To analyze how geometric modifications impact airfoil efficiency, simulations were performed using XFLR5 (v7.56). XFLR5 is an analysis tool for airfoils, wings, and planes operating at low Reynolds Numbers; or in other words, low-speed velocities. Flow5, which is Version 7 of the software, was released to be open-source on January 1st, 2026. It includes the Direct and Inverse analysis capabilities of XFoil and wing design and analysis capabilities based on the Lifting Line Theory, the Vortex Lattice Method, and on a 3D Panel method [16].

A standardized numbering system was established to keep track of and organize a large volume of modified airfoil geometries tested through XFLR. The control group (1.0 Series) was the NACA 2412, which served as a benchmark for all comparative analysis.

Each integer designated the main geometric variable that was being modified from the baseline control airfoil. For instance, the 2.0 series encompassed all versions of airfoils where the mean camber was altered, while subsequent integer groups represented variations in other variables such as thickness. Decimal increments (2.1, 2.2, 2.3, etc.) represented individual variations within that specific category.

The NACA 2412 was selected as the control airfoil due to its reputation as a benchmark in general aviation and aerodynamics. It features a moderate 2% max camber located at 40%

chord and a 12% maximum thickness. It is also the most thoroughly documented airfoil in historical NACA reports, and is widely used in standard light aircraft structures such as the Cessna 172 [17]. Thus, using the NACA 2412 as the control group airfoil established a reliable reference point against which the advantages and disadvantages of geometric modifications could be accurately measured.

All boundary layer and environmental simulation parameters were kept constant throughout each analysis run. All airfoils were evaluated using a Direct Foil Analysis, maintaining a fixed Reynolds number sweep, kinematic viscosity, and uniform air density.

The variables changed were:

1. Mean Camber
2. Position of Maximum Camber
3. Maximum Thickness
4. Position of Maximum Thickness

Results/Discussion |

The primary objective of this investigation was to identify the geometric airfoil modifications that maximize the Lift-to-Drag ratio (C*l* / C*d*) as well as the peak lift capability (C*l* max) for low-speed flight.
Optimizing these variables is crucial for STOL-capable flights since the aircraft would be able to generate higher aerodynamic lift at lower forward speeds, allowing it to liftoff on shorter runways and gain the altitude needed to clear obstacles. By reducing the drag force while generating more lift, the aircraft would also require less engine power and time spent operating at full-throttle, directly reducing total carbon emissions during take-off.

To evaluate whether a modified airfoil outperformed the NACA 2412 (control group), three primary metrics from the XFLR graphs were analyzed:

1. Maximized Lift-to-Drag Ratio: As explained earlier, it is incredibly crucial for STOL-capable aircrafts to have a maximized L/D ratio. A high L/D ratio across relevant angles of attack (α = 4°to 10°) would ensure that the wing produces sufficient lift without creating severe aerodynamic drag penalties.
2. Maximum Lift Coefficient: A higher C*l* max value directly relates to better liftoff capability in low-speed.
3. Minimal Stall Behavior at Lower Speeds: This was a qualitative measure evaluated by the slope of the lift curve after the C*l* max. Graphs with gradual stall characteristics are considered better than those with sharp ‘cliff’-like changes (which exhibit severe flow separation).

Airfoil 1.0 (Control):

Specifics:
Thickness: 12.00 % at 29.03%
Camber: 2% at 39.54%
Points: 99
TE Flap: 0 degree
TE XHinge: 0
TE YHinge: 0

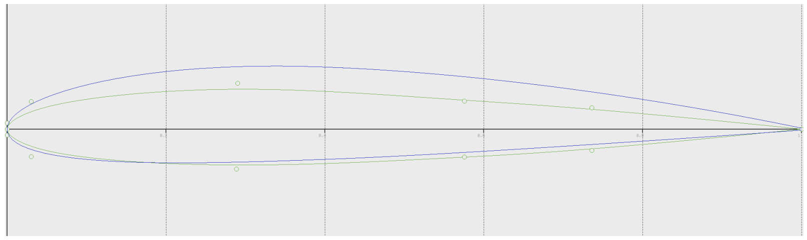

Figure 10: NACA 2412 (Control) Airfoil

Cl vs Cd

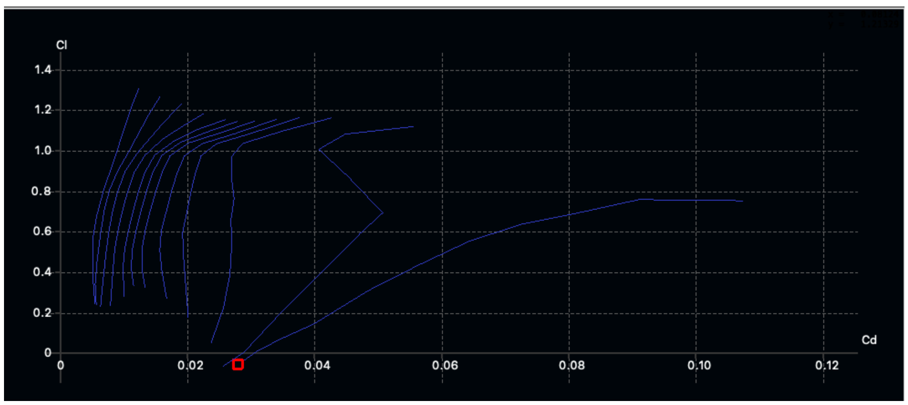

Figure 11: Airfoil 1.0 Cl vs Cd Plot; x-axis represents coefficient of drag, and y-axis represents coefficient of lift.

Cl/Cd vs Alpha

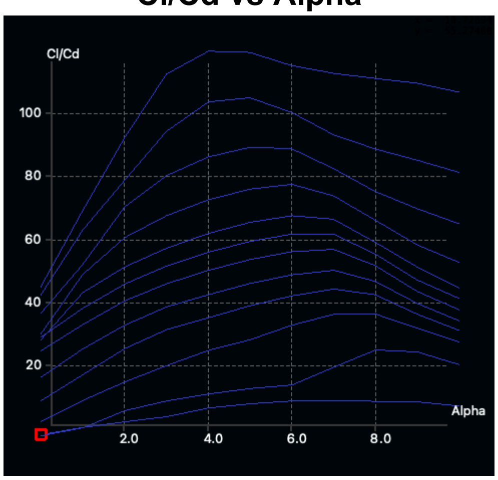

Figure 12: Airfoil 1.0 Cl/Cd vs Alpha plot; x-axis is angle of attack (degrees), y-axis is Cl/Cd

Cl vs Alpha

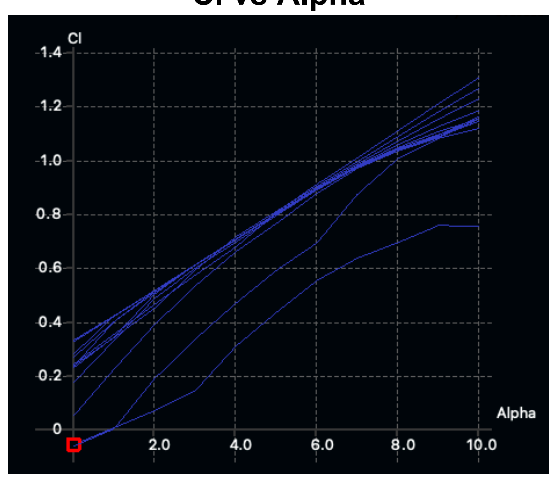

Figure 13: Airfoil 1.0 Cl vs Alpha plot; x-axis is angle of attack (degrees), y-axis is Cl

The C*l* vs C*d* graph reveals that as the Reynolds number increased, the drag curves shifted toward a significantly steeper, almost vertical trajectory on the left side of the graph. This near-vertical trajectory indicates that at higher speeds (higher Reynolds number values), the airfoil achieves significant lift with a minimal drag penalty.

On the other hand, at lower speeds, the airfoil showcases a flatter slope, with the curves shifting far to the right, suggesting a lower L/D ratio.

Across all the simulated Reynolds numbers, however, the slope of the lines break pattern and begin to flatten out once the lift coefficient exceeds 1.0, with the curves shifting far right and exhibiting non-linear “zigzag” trajectories. This behavior demonstrates boundary layer separation and the formation of a Laminar Separation Bubble, where the laminar flow across the airfoil detaches from the surface due to the adverse pressure gradient (moving from low pressure to high pressure).

From the C*l*/C*d* vs Alpha graph, it can be observed that the maximum L/D ratio amounted to 120 at the highest tested Reynolds number at Alpha = 4 degrees. Beyond this point, however, the efficiency degrades since the drag increases faster than the lift production.

For the lower Reynolds numbers (lower speeds), the efficiency curves broaden, and their peaks shift to the right, reaching maximum C*l*/C*d* values at higher angles of attack (6° - 8°). At the lowest airspeeds, peak efficiency drops below $(Cl/Cd)_{max} = 20$.

In the C*l* vs Alpha plot, it can be observed that the high Reynolds number curves showcase a constant, mostly linear slope across low angles of attack (0° - 6°).

For the lowest Reynolds number curve, boundary layer separation occurs much earlier, with the line stalls around 9°. At this point the line plateaus at C*l* ≈ 0.75.

The highest coefficient of lift is 1.32 for the highest Reynolds number, occurring at an angle of attack of 10°.

Airfoil 2.0:

Specifics:
Thickness: 12.00 % at 29.03
Camber: 4% at 39.54%
Points: 99
TE Flap: 0 degree
TE XHinge: 0
TE YHinge: 0

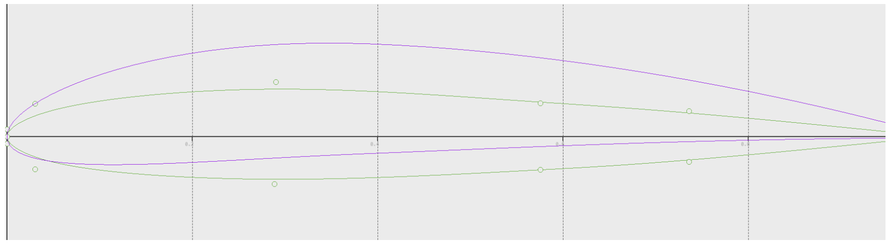

Figure 14: Airfoil 2.0 (Camber Increased by 2%)

Cl vs Cd

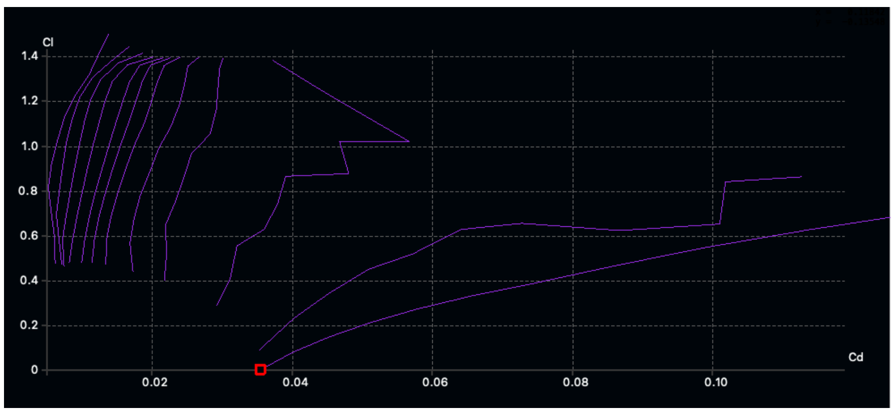

Figure 15: Airfoil 2.0 Cl vs Cd Plot; x-axis represents coefficient of drag, and y-axis represents coefficient of lift.

Cl/Cd vs Alpha

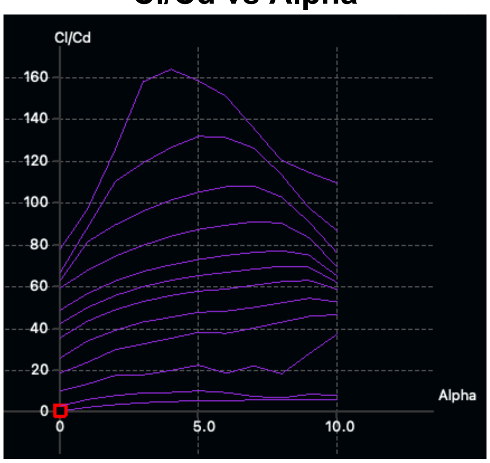

Figure 16: Airfoil 2.0 Cl/Cd vs Alpha plot; x-axis is angle of attack (degrees), y-axis is Cl/Cd

Cl vs Alpha

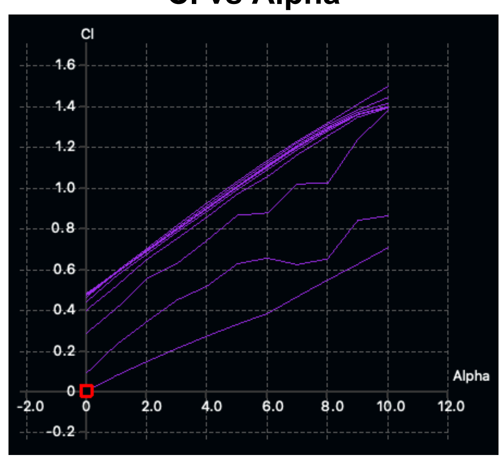

Figure 17: Airfoil 2.0 Cl vs Alpha plot; x-axis is angle of attack (degrees), y-axis is Cl

In this airfoil, the camber was increased from 2% to 4%. Once again, the lower Reynolds number curves on the C*l* vs C*d* graph exhibit more jagged trajectories than the higher speed curves.

For higher Reynolds numbers, the curves shift vertically along the y-axis without a corresponding horizontal (drag) penalty. The maximum coefficient of lift increased to being 1.35. This confirms that an increased camber generates significant lift without increasing the initial profile drag during the early ground acceleration period.

At the lowest Reynolds number values, the curves maintain 'step-like', jagged trajectories between C*l* = 0.6 and C*l* = 1.0. This indicates that while an increased camber does enhance C*l*/C*d* performance, low-speed flow still struggles with laminar boundary layer separation. This makes intuitive sense as well, since a more curved airfoil shape would result in a steeper surface for the airflow to follow.

The maximum C*l*/C*d* has increased by 33% - from 120 to a little 160, whereas the optimal angle of attack remained at 4 degrees. The highest coefficient of lift also increased, going from 1.3 to 1.5. This shows how increasing the mean camber line can increase L/D efficiency for STOL aircrafts.

However, when the camber was increased to 9%, pressure drag was created. At extreme camber, though C*l* did increase slightly, the coefficient of drag increased exponentially (due to early boundary layer separation). This leads to the overall L/D ratio collapsing.

Slightly shifting the location of the maximum camber along the chord length has little effect on the performance of the airfoil (emphasis on slightly). However, major shifts can result in different graph results.

For instance, when the peak camber was moved further back towards the trailing edge, the maximum coefficient of lift was lowered and the airfoil stalls more sharply at higher angles of attack.

On the other hand, a more forward camber position can increase low-speed maximum lift and result in a gentler and more progressive stall - which is perfect for STOL-capable aircrafts since they must be able to takeoff at lower speeds than commercial aircrafts.

Airfoil 3.0:

Specifics:
Thickness: 16.00 % at 29.03%
Camber: 2% at 39.54%
Points: 99
TE Flap: 0 degree
TE XHinge: 0
TE YHinge: 0

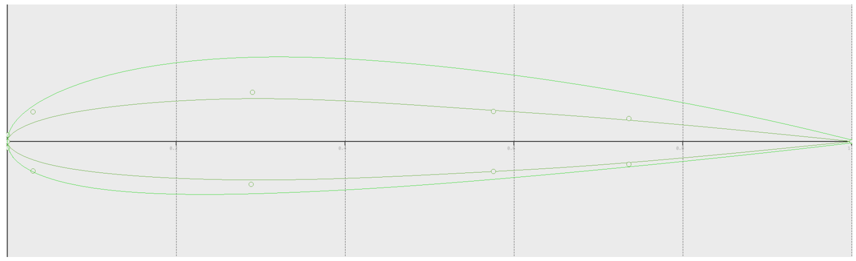

Figure 18: Airfoil 3.0 (Thickness Increased by 4%)

Cl vs Cd

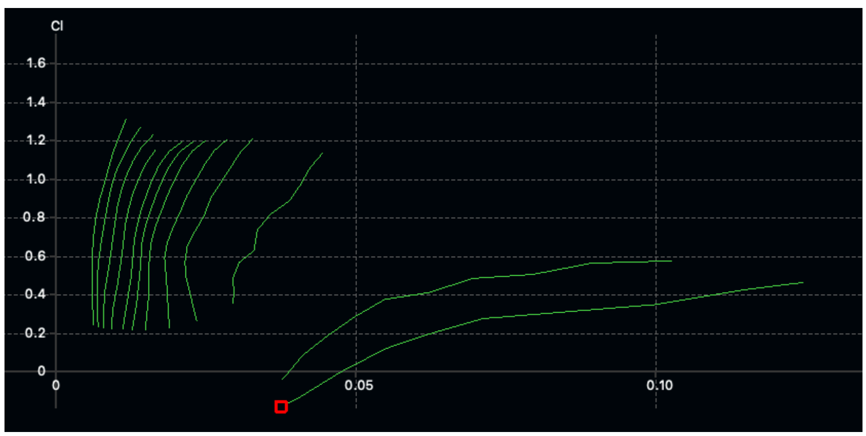

Figure 19: Airfoil 3.0 Cl vs Cd Plot; x-axis represents coefficient of drag, and y-axis represents coefficient of lift.

Cl/Cd vs Alpha

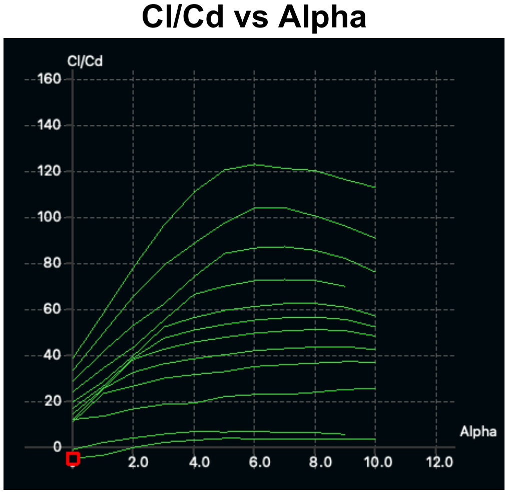

Figure 20: Airfoil 3.0 Cl/Cd vs Alpha plot; x-axis is angle of attack (degrees), y-axis is Cl/Cd

Cl vs Alpha

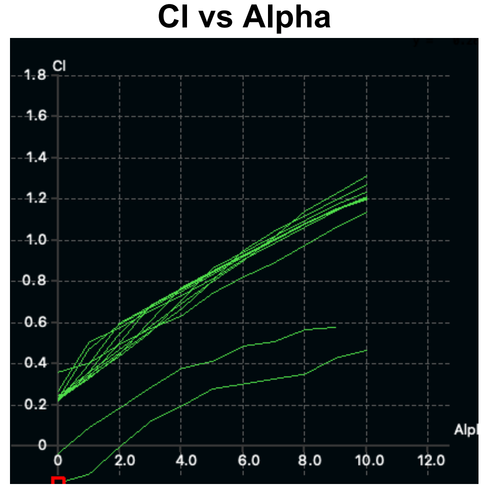

Figure 21: Airfoil 3.0 Cl vs Alpha plot; x-axis is angle of attack (degrees), y-axis is Cl

In Airfoil 3.0, the maximum thickness was increased from 12% to 16%. This significantly altered the drag force, particularly at lower Reynolds numbers.

In the C*l* vs C*d* plot, the lowest two Reynolds number curves detached substantially from the main trend, highlighting that at lower speeds an airfoil with an increased thickness imposes a significant drag penalty. This would prove to be a hindrance to STOL aircrafts that must start off at a lower speed in takeoff.

For higher speeds, however, the peak for the C*l*/C*d* is 125 at an angle of attack of 6°, as seen in the C*l*/C*d* vs Alpha plots. This value is slightly higher than the NACA 2412's (Airfoil 1.0) maximum C*l*/C*d* of 120 at an approximately 4° angle of attack.

It is important to note that the maximum L/D ratio can be achieved at a greater angle of attack for Airfoil 3.0, since STOL aircrafts are required to clear taller, larger obstacles on the ground during the climb-out phase.

The maximum lift coefficient is 1.3 less than that of Airfoil 2.0's at 1.5, and is 0.02 less than Airfoil 1.0's Cl_{max} of 1.32. So not only is the airfoil with greater thickness inefficient in terms of C*l*/C*d* for lower speeds, but it also fails to generate a greater maximum lift when compared to the control group.

Despite the lower Cl_{max}, the top of the lift curves bend gradually instead of dropping suddenly. This behaviour indicated a progressive trailing-edge stall, which can provide STOL pilots with a broader margin of safety against sudden stall during abrupt maneuvers.

Moving the placement of the maximum thickness along the chord line to the front of the airfoil proves to be very beneficial for STOL performance. It generates a higher C*l* max and also results in a gentler, more gradual stall.

Conclusion |

In summary, geometric modifications evaluated across airfoils demonstrated that mean camber increase provides the most significant aerodynamic gains for STOL operations. Doubling the camber increased peak efficiency by 33% and boosted maximum lift capacity.

Conversely, changing thickness in isolation introduced a higher drag penalty at lower Reynolds numbers (lower speeds) and resulted in a lower maximum lift generation. However, moving the placement of both maximum camber and maximum thickness towards the leading edge of the airfoil helps in reducing drastic stall and increases Cl max value as well, which is very beneficial to STOL-capable flight.

These results, when implemented in airfoils, will allow STOL aircrafts to takeoff at lower ground airspeeds and shorter runways. This ultimately curtails the time spent in takeoff ground roll, which is the phase where the aircraft engines operate at maximum fuel consumption rates. By reducing the duration of full-throttle fuel burn, optimized airfoil geometries lower the overall fuel burn per STOL flight departure, which ultimately furthers the broader aviation decarbonization goals.

References:

[1] Ritchie, Hannah. “What Share of Global CO_2 Emissions Come from Aviation?” *Our World in Data*, Apr. 2024, https://ourworldindata.org/global-aviation-emissions.

[2] Aviation International News. “Does eSTOL Hybrid Power and Blown Lift Beat Vertical Powered Lift? – FutureFlight.” YouTube, 15 Nov. 2022, https://www.youtube.com/watch?v=PjdmNp-xL3U.

[3] The Green Aircraft Concept - CLIMATE FRIENDLY LONG RANGE AIRCRAFT. 15 Oct. 2021, https://green-aircraft.com/.

[4] “Short Take-Off and Landing (STOL) | SKYbrary Aviation Safety.” Skybrary.Aero, https://skybrary.aero/articles/short-take-and-landing-stol.

[5] Diekmann, J. H. “Flight Mechanical Challenges of STOL Aircraft Using Active High Lift.” AIAA Aerospace Research Center, 10 Aug 2019, https://arc.aiaa.org/doi/10.2514/1.C034910

[6] National Aviation Academy. “Airfoil Design 101: What Is an Airfoil?” National Aviation Academy, 14 Mar. 2022, https://www.naa.edu/airfoil-design/.

[7] *(Figure 1)* “Lift.” Code7700.Com, https://code7700.com/lift.htm.

[8] Nakamura, Mealani. “How An Airfoil Works.” Mit.Edu, 1999, https://web.mit.edu/2.972/www/reports/airfoil/airfoil.html.

[9] *(Figures 3, 4, 5, 6, 7, 8)* SIMSCALE. “What Is Lift, Drag and Pitch?” SimScale, 1 Sept. 2023, https://www.simscale.com/docs/simwiki/lift-drag-pitch/.

[10] *(Equation 1)* Princeton University. “Bernoulli’s Equation.” Princeton.Edu, 2019, https://www.princeton.edu/~asmits/Bicycle_web/Bernoulli.html.

[11] *(Figure 9)* Benson, Tom. “L/D Ratio.” Www.Grc.Nasa.Gov, https://www.grc.nasa.gov/www/k-12/VirtualAero/BottleRocket/airplane/ldrat.html.

[12] Bousman, William. Airfoil Design and Rotorcraft Performance. https://rotorcraft.arc.nasa.gov/Publications/files/Bousman_AHSF02.pdf.

[13] *(Equation 2)* Benson, Tom. “The Lift Coefficient.” Www.Grc.Nasa.Gov, https://www.grc.nasa.gov/www/k-12/VirtualAero/BottleRocket/airplane/liftco.html.

[14] Bravo-Mosquera, Pedro. “Design and aerodynamic evaluation of a medium STOL tactical transport aircraft.” Www.sagepub.com, https://www.researchgate.net/profile/Hernan-Ceron-M/publication/352127793_Design_and_aerodynamic_evaluation_of_a_medium_short_takeoff_and_landing_tactical_transport_aircraft/links/60ba2ecd299bf10dff96d89b/Design-and-aerodynamic-evaluation-of-a-medium-short-takeoff-and-landing-tactical-transport-aircraft.pdf

[15] *(Equation 3)* “Forces in a Climb.” Www.Grc.Nasa.Gov, https://www.grc.nasa.gov/www/k-12/VirtualAero/BottleRocket/airplane/climb.html.

[16] “Xflr5.” Flow5.Tech, 2026, https://www.flow5.tech/xflr5/xflr5.html.

[17] Ali, Md. Rafayet Bin, and Tammem Hasan. “Comparative Numerical Analysis of NACA 2412, NACA 0012, and NACA 63-412 Airfoil Performance for Cessna 172 Aircraft Wings.” SciEn Conference Series: Engineering, vol. 3, Nov. 2025, pp. 377–82, https://doi.org/10.38032/scse.2025.3.104.